J. Fluid Mech. (1994), *vol.* 262, *pp.* 325–351

On the high-Rayleigh-number structure of steady laminar natural-convection flow in a square enclosure

By M. R. RAVI†, R. A. W. M. HENKES‡ AND C. J. HOOGENDOORN

Faculty of Applied Physics, Delft University of Technology, PO Box 5046, 2600 GA Delft, The Netherlands.

(Received 7 October 1992 and in revised form 11 May 1993)

Natural-convection flow in an enclosure with adiabatic horizontal walls and isothermal vertical walls maintained at a fixed temperature difference has been investigated. At high values of the natural-convection parameter, the Rayleigh number, a recirculating pocket appears near the corners downstream of the vertical walls, and the flow separates and reattaches at the horizontal walls in the vicinity of this recirculation. There is also a considerable thickening of the horizontal layer. In some previous studies by different authors, this corner flow was considered to be caused by an internal hydraulic jump, and the jump theory was used to predict bifurcation of the steady flow into periodic flow. The present work examines the corner phenomenon closely to decide if it is indeed caused by a hydraulic jump. The results of the analysis reveal the oversimplification of the problem made in the previous studies: there is no connection of the corner phenomenon with a hydraulic jump. The separation of flow at the ceiling is not a feature of hydraulic jumps, and the essential energy loss associated with hydraulic jumps is not observed in the corner flow. It is shown that the corner structure is caused by thermal effects. Owing to the temperature undershoots in the vertical boundary layer, which are known to be caused by the stable thermal stratification of the core, relatively cold fluid reaches the upper corner. This cold fluid detaches from the ceiling like a plume at high Rayleigh numbers, and causes the separation and recirculation.

1. Introduction

Natural-convection flow inside a square enclosure with differentially heated vertical walls and adiabatic horizontal walls is a classical heat-transfer problem. It has a wide variety of technical applications, such as in cooling of electronic equipment, climatic conditioning of rooms, cooling of nuclear reactors, solar collectors, etc. It is also a test case for new computer programs, and has been benchmarked by several authors (de Vahl Davis 1983; Le Quéré 1991). At high values of the natural-convection parameter, the Rayleigh number (*Ra*), the flow structure inside the enclosure shows interesting patterns (Chenoweth & Paolucci 1986; Le Quéré 1987; Paolucci & Chenoweth 1989; Henkes 1990): for increasing Rayleigh number, the steady solution bifurcates to an

† Present address: FAST, URA-871, CNRS, Bâtiment 502, 91405 Orsay, France.
‡ Present address: Faculty of Aerospace Engineering, Delft University of Technology, PO Box 5058, 2600 GB Delft, The Netherlands.

unsteady periodic solution, transforms into a chaotic solution, and finally becomes fully turbulent.

The present work considers the flow structure in the enclosure in the steady flow regime, at Rayleigh numbers just below the critical Rayleigh number for bifurcation to an unsteady state. At such large Rayleigh numbers, the flow is characterized by thin vertical boundary layers adjacent to the vertical walls, a thermally stratified core, boundary layers adjacent to the horizontal walls and corner regions. For air, the flow in the corner region shows a recirculating pattern and a separation at the horizontal walls at high Rayleigh numbers prior to bifurcation. For water, no such recirculation or separation is observed. Different existing studies (Le Quéré 1987; Paolucci & Chenoweth 1989; Henkes & Hoogendoorn 1990) considered that the sudden expansion of the flow along the horizontal wall downstream of the recirculation region is analogous to an internal hydraulic jump.

The basic reason for relating the flow structure in the corner region of an enclosure to an internal hydraulic jump is rather historical. Ivey (1984) suggested that a specific oscillatory behaviour that he observed in his experiments during the initial transients of the flow of water in a square enclosure, when the temperature difference was suddenly imposed on the vertical walls, could have been caused by an internal hydraulic jump. His suggestions are worded in a speculative language, and are based only on the wave-like appearance of the transient flow structure. Based on the scalings of the vertical boundary layers, he derived an expression for the characteristic Froude number for this proposed internal hydraulic jump, as a function of the Rayleigh and Prandtl numbers. Patterson & Armfield (1990) and Armfield & Patterson (1991) strongly refuted the suggestions of Ivey (1984) as 'conjecture' and showed through experimental and computational means that it is not an internal hydraulic jump that is responsible for this oscillatory flow, but it is the pressure-wave action caused by the splitting of the horizontal intrusions reaching the vertical wall on the opposite side of the enclosure.

Nevertheless, the extension of the scaling arguments of Ivey (1984) to the steady-state conditions of the flow of air in a square enclosure by Paolucci & Chenoweth (1989) predicted the Rayleigh number of bifurcation for air reasonably well. In the present work, it is proposed to consider this proposition, and verify its correctness. It is intended to carry out an in-depth analysis of the flow near the corner of an enclosure at high Rayleigh numbers in the steady flow regime, with a view to examining whether the flow structure could indeed be characterized by internal hydraulic jump theory.

2. Mathematical formulation

The problem under consideration involves the steady flow of air due to natural convection in a square enclosure, caused by differentially heated vertical walls and insulated horizontal walls. This geometry is shown in figure 1. The enclosure has sides of length H. The hot vertical wall on the left is kept at a temperature T_h and the cold vertical wall on the right is kept at a temperature T_c. The directions of the acceleration due to gravity g and the coordinate axes are also shown in figure 1.

The flow in the above problem is assumed to be two-dimensional and incompressible, with density variation only in the body force term, according to the Boussinesq approximation. Fluid properties are assumed to be constant. Pressure work and viscous dissipation are neglected in the energy equation. The governing equations can

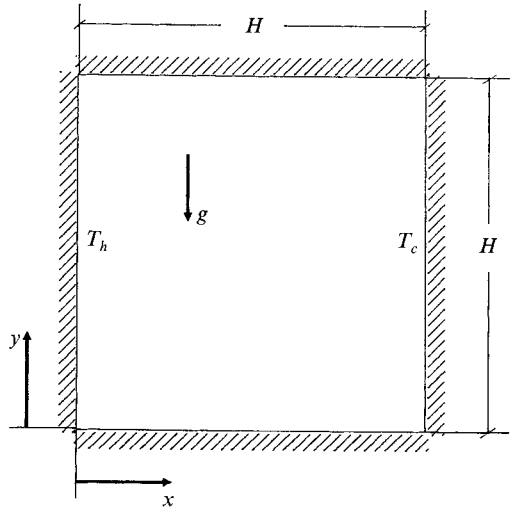

FIGURE 1. Geometry of computational domain.

be written as follows:

$$\frac{\partial u}{\partial x} + \frac{\partial v}{\partial y} = 0, \tag{2.1}$$

$$\frac{\partial u}{\partial t} + u\frac{\partial u}{\partial x} + v\frac{\partial u}{\partial y} = -\frac{1}{\rho_{ref}}\frac{\partial p_d}{\partial x} + \nu\left(\frac{\partial^2 u}{\partial x^2} + \frac{\partial^2 u}{\partial y^2}\right), \tag{2.2}$$

$$\frac{\partial v}{\partial t} + u\frac{\partial v}{\partial x} + v\frac{\partial v}{\partial y} = -\frac{1}{\rho_{ref}}\frac{\partial p_d}{\partial y} + g\beta(T - T_{ref}) + \nu\left(\frac{\partial^2 v}{\partial x^2} + \frac{\partial^2 v}{\partial y^2}\right), \tag{2.3}$$

$$\frac{\partial T}{\partial t} + u\frac{\partial T}{\partial x} + v\frac{\partial T}{\partial y} = \alpha\left(\frac{\partial^2 T}{\partial x^2} + \frac{\partial^2 T}{\partial y^2}\right), \tag{2.4}$$

where u and v are the velocity components in the x- and y-directions respectively, t is the time, T is the temperature, ρ is the density, ν and α are the kinematic viscosity and the thermal diffusivity of the fluid respectively, g is the acceleration due to gravity and β is the coefficient of cubical thermal expansion. The density is assumed to be equal to a constant reference density ρ_{ref} in all the terms other than the body force term in equation (2.3). p_d is the pressure difference defined as

$$p_d(x, y) = p(x, y) - \rho_{ref} g(y - y_{ref}),$$

where y_{ref} is an arbitrary reference datum.

The boundary conditions for the above system of equations corresponding to the geometry in figure 1 can be written as follows:

$x = 0$:	$u = 0$;	$v = 0$;	$T = T_h$,
$x = H$:	$u = 0$;	$v = 0$;	$T = T_c$,
$y = 0$:	$u = 0$;	$v = 0$;	$\partial T/\partial y = 0$,
$y = H$:	$u = 0$;	$v = 0$;	$\partial T/\partial y = 0$.

These governing equations can be non-dimensionalized using the length H of the enclosure sides as the reference length, the Brunt–Väisälä velocity scale $u_B = (g\beta\Delta T H)^{\frac{1}{2}}$ as the reference velocity, $T_{ref} = (T_h + T_c)/2$ as the reference temperature

$(g\beta\Delta T H)^{\frac{1}{2}}$ as the reference velocity, $T_{ref} = (T_h + T_c)/2$ as the reference temperature and $\Delta T = (T_h - T_c)$ as the reference temperature difference. This gives rise to two non-dimensional parameters: the Rayleigh number $Ra = (g\beta\Delta T H^3)/(\nu\alpha)$ and the Prandtl number $Pr = \nu/\alpha$. The flow field in the enclosure is entirely a function of these two parameters.

The system of non-dimensionalized equations is integrated over control volumes for the respective variables on a staggered grid to arrive at the discretized algebraic equations for the variables at their grid points. A fourth-order symmetric central difference scheme has been used for the advection terms and a second-order central difference scheme has been used for the diffusion terms. The details of the discretization procedure are presented by Janssen & Henkes (1993). The solutions are marched in time to obtain the steady-state results. Most of the computations for the present analysis were performed on an 80×80 non-uniform grid. For higher Rayleigh numbers, grid independence of results required a finer grid, and the computations were performed on a 120×120 or a 240×240 non-uniform grid. A grid refinement from 120×120 to 240×240 grid points for air at $Ra = 10^8$ results only in less than 0.2% change in the characteristic quantities, such as the average wall heat transfer, maximum values of the horizontal and vertical velocity components and the gradient of the temperature stratification at the centre of the enclosure.

In all the solutions obtained, the flow exhibits a symmetry about the centre of the enclosure. In the forthcoming discussion, we shall concentrate on the flow structure at the top left corner. Owing to the symmetry, the description would be valid for the bottom right corner also.

3. Evolution of flow structure

3.1. *Effect of Rayleigh number*

In order to understand the behaviour of the flow in the corner region at high Rayleigh numbers, let us look at how the flow structure of air ($Pr = 0.71$) evolves in an enclosure for increasing Rayleigh number. Figure 2(*a–e*) shows the streamline patterns for air at Rayleigh numbers of 10^4, 10^5, 10^6, 10^7 and 10^8 respectively. At a Rayleigh number of 10^4 (figure 2*a*), the flow shows a single clockwise cell in the enclosure. As the Rayleigh number is increased to 10^5, the streamlines move closer to the vertical walls (figure 2*b*). On further increase in Rayleigh number, the streamlines in the core region become more or less horizontal and the streamlines which crowd near the vertical walls start forming a boundary layer at these walls (figure 2*c*). Boundary layers are also formed adjacent to the horizontal walls of the enclosure. The flow near the corner now starts spreading out into the interior more sharply, giving rise to more or less a *sudden expansion* or a *jump-like* structure.

Taking a closer look at the flow near the corner with increasing Rayleigh number, one can see that the flow spreads from a thin layer to cover most of the half-width of the enclosure, sharply after it negotiates the turn at the corner. As this turn becomes sharper, a pocket of fluid forms, getting trapped between the upcoming boundary layer on one side and the flow spreading into the interior of the enclosure on the other side. This pocket evolves into a recirculation region at Rayleigh numbers between 10^6 and 10^7 (figure 2*d*,*e*). As the turn and the expansion sharpen further, the flow separates at the horizontal wall, and reattaches itself after the spreading. The separation zone is seen to form at around $Ra = 10^7$ (figure 2*d*), and is seen clearly at $Ra = 10^8$ (figure 2*e*).

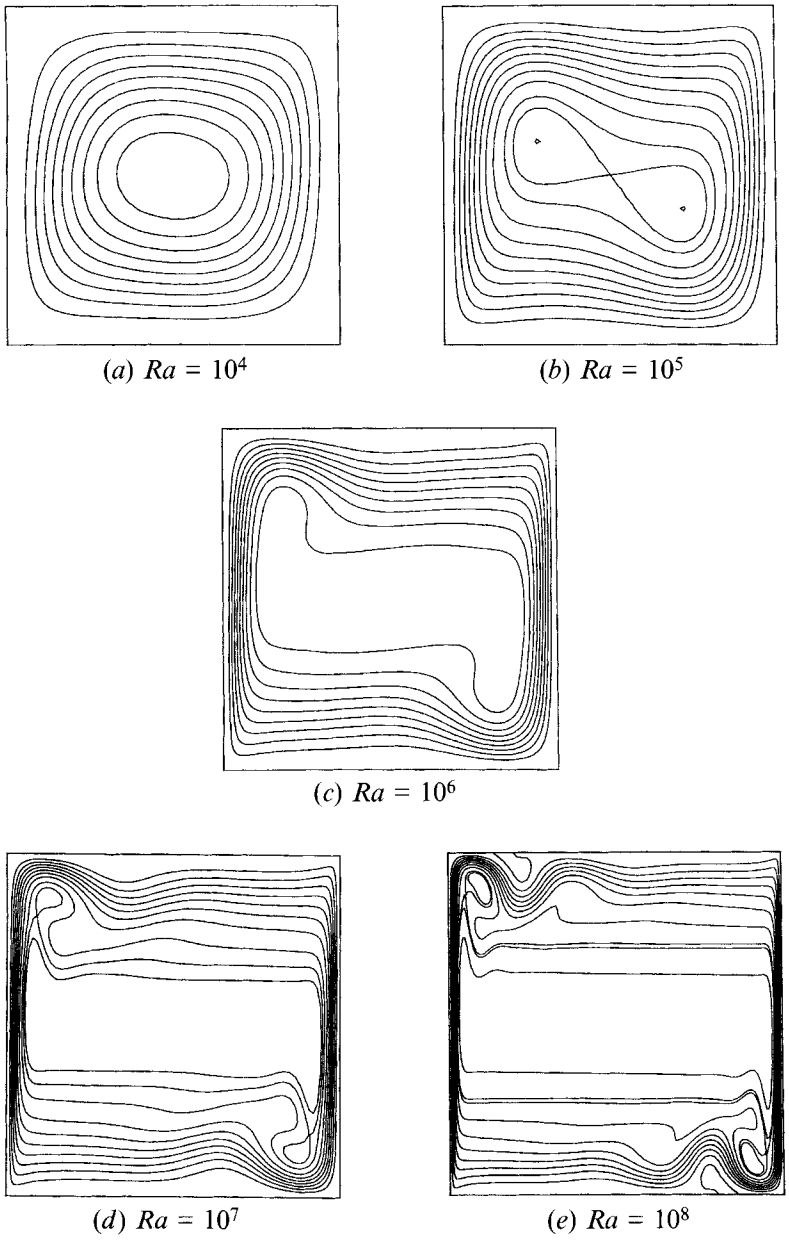

(*a*) $Ra = 10^4$ (*b*) $Ra = 10^5$

(*c*) $Ra = 10^6$

(*d*) $Ra = 10^7$ (*e*) $Ra = 10^8$

FIGURE 2. Evolution of flow structure with Rayleigh number at $Pr = 0.71$.

The occurrence of a recirculating pocket now clearly demarcates the flow in the enclosure into two streams: one flowing close to the walls, through the vertical and horizontal wall layers, and undergoing the sudden expansion; the other simply going around the central region of the enclosure without reaching the walls. Figure 3 shows the streamline that demarcates the two streams, at a Rayleigh number of 10^8 and Prandtl number of 0.71. This streamline passes through the nodal point where the recirculating loop at the corner region touches the recirculating loop in the central region. This special streamline will be referred to as the *dividing streamline*, in the

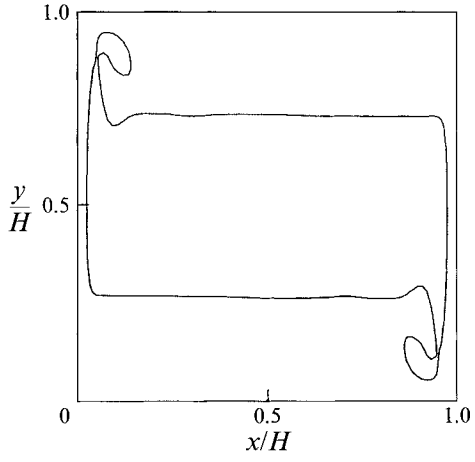

FIGURE 3. Dividing streamline at $Ra = 10^8$ and $Pr = 0.71$.

forthcoming discussion. The dividing streamline thus divides the flow into the *wall region* and the *interior region.*

3.2. *Effect of Prandtl number*

To understand the effect of Prandtl number on the flow structure, specifically with reference to the corner recirculation and the separation at the horizontal wall, computations were performed for a Rayleigh number of 10^8, gradually increasing the Prandtl number. For water ($Pr = 7.0$), the recirculation region in the corner does not appear even for Rayleigh numbers as high as 10^{10}. The accuracy of this computation was verified by grid refinement up to a 320×320 non-uniform grid. For Prandtl numbers of 4.0 and even 2.0, there were no signs of the recirculation pattern at $Ra = 10^9$. So, it was decided to close in on the range of Prandtl numbers between 0.71 and 2.0 in order to investigate the effect of Prandtl number on the corner recirculation and the separation at the wall.

Figure 4 shows the evolution of the flow structure with an increase in Prandtl number. It can be observed that at a given Ra, while the thickness of the boundary layers at the vertical walls remains almost unaltered, the corner recirculation zone and the separation zone gradually shrink and disappear as Prandtl number is increased. For $Ra = 10^8$, the separation zone ceases to exist when Pr exceeds 1.2, while the recirculation region disappears for Pr exceeding 1.4.

4. Scaling of corner flow

The high-Rayleigh-number corner flow for air consists of two distinct phenomena: the recirculation and the separation at the ceiling. For air, the recirculation commences when the Rayleigh number exceeds 10^6, and the flow separates at the ceiling for $Ra > 10^7$. For water ($Pr = 7.0$), the recirculation zone does not appear even at very high values of Rayleigh number. The evolution of flow at $Ra = 10^8$ with increasing Prandtl number showed that the separation at the wall ceases to exist for $Pr > 1.2$, while the recirculation zone in the corner vanishes for $Pr > 1.4$. In order to study the dependence of these two phenomena on the Rayleigh number and Prandtl number, computations were carried out for $Pr = 0.85$, 1.0, 1.2, 1.4 and 1.6, at various Rayleigh numbers in the steady flow regime. The results are used to scale the evolution of the

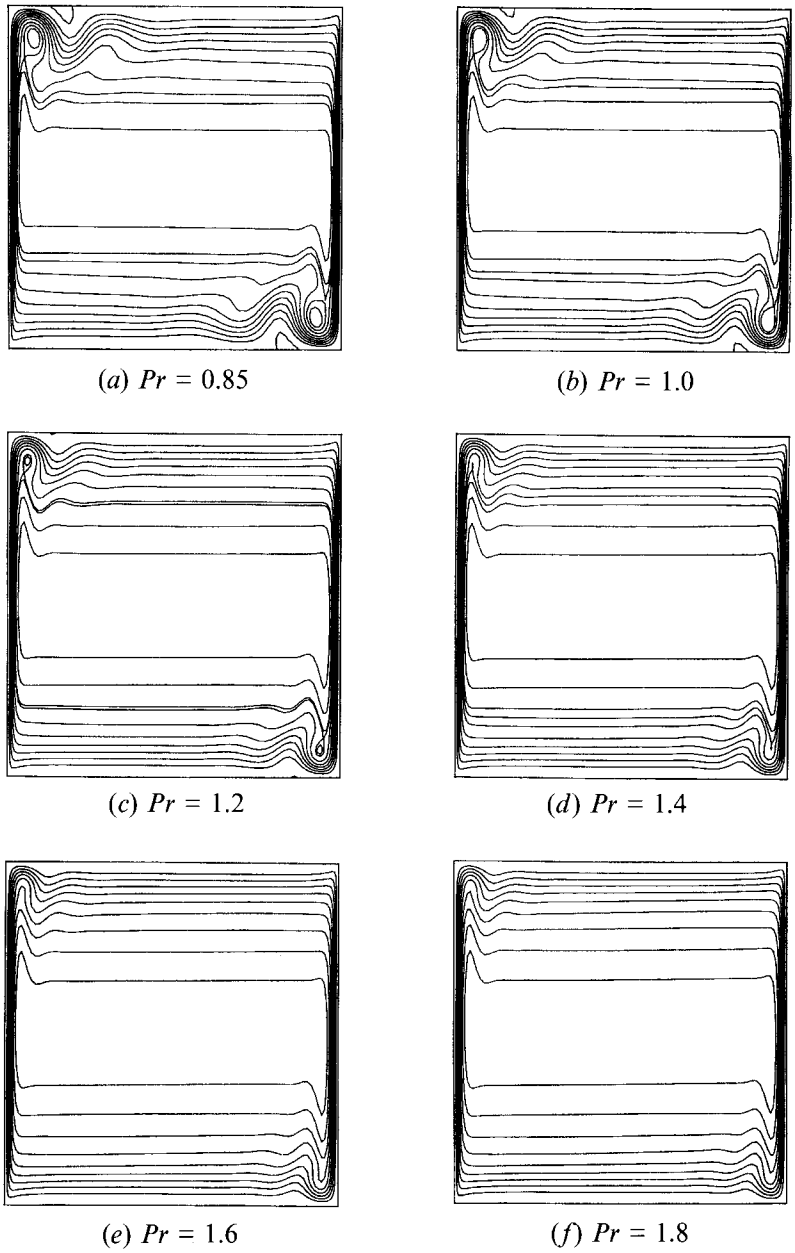

(*a*) $Pr = 0.85$ (*b*) $Pr = 1.0$

(*c*) $Pr = 1.2$ (*d*) $Pr = 1.4$

(*e*) $Pr = 1.6$ (*f*) $Pr = 1.8$

FIGURE 4. Evolution of flow structure with Prandtl number at $Ra = 10^8$.

corner flow phenomena as functions of Rayleigh and Prandtl numbers. A comparison of these scalings is made with those based on the theory of the internal hydraulic jump, due to Paolucci & Chenoweth (1989).

4.1. *Computed scaling of corner flow*

For this comparison, it is important to accurately identify the point of commencement of the recirculation from the computed data. A visual comparison of the streamline plots and the stagnant point locations provides an idea of the range of Rayleigh numbers at which the recirculation zone commences. Computations are performed

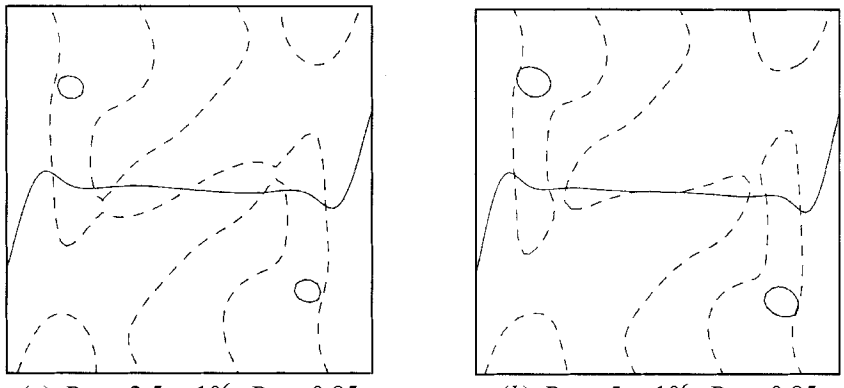

(*a*) $Ra = 2.5 \times 10^6$; $Pr = 0.85$ (*b*) $Ra = 5 \times 10^6$; $Pr = 0.85$

FIGURE 5. Determining commencement of recirculation: contours of $u = 0$ (——) and $v = 0$ (- - - -).

at smaller intervals of Rayleigh number in this probable range in order to pinpoint the Rayleigh number of commencement of the recirculation zone, for a given Prandtl number. Sample cases are illustrated to describe the methodology adopted to identify the points of commencement of the recirculation and separation zones from the numerical results.

Figures 5(*a*) and 5(*b*) show the intersection of the velocity contours $u = 0$ and $v = 0$ for $Pr = 0.85$. Figure 5(*a*) corresponds to $Ra = 2.5 \times 10^6$ and figure 5(*b*) corresponds to $Ra = 5 \times 10^6$. It can be seen that near the corner, the contours of $u = 0$ and $v = 0$ do not intersect at $Ra = 2.5 \times 10^6$, whereas they do intersect to give rise to two stagnant points at $Ra = 5 \times 10^6$. In order to narrow down the probable range of Ra values within which the commencement point occurs, computations were performed for some more values of Ra in the above range. A logarithmic mean of the narrowed-down range of Ra values was used as the point of commencement of recirculation. The same procedure was followed for all the values of Prandtl number investigated. The observed data were fitted by a least-squares fit to a power-law relation with Prandtl number, to obtain the following equation:

$$Ra_r = 10^{6.9987} Pr^{6.1052}.$$

The exponent of the Prandtl number in the above relation was rounded off, and the constant was redetermined corresponding to the new exponent, in the range of Prandtl numbers investigated. This gives

$$Ra_r = 10^7 Pr^6 \tag{4.1}$$

for all the Prandtl numbers investigated, in the range of 0.71 to 1.6.

Flow separation and reattachment points are characterized by zero velocity gradients normal to the surface, i.e. zero shear stress at the wall. This character is used to locate the separation and reattachment points, and to determine the Rayleigh number at which the flow separation commences for a given Prandtl number. Figure 6 shows the non-dimensional wall shear stress at the ceiling, for $Ra = 10^{7.75}$ and 10^8, at $Pr = 1.2$. It is seen that the curve for $Ra = 10^{7.75}$ does not touch the zero line, while the curve for $Ra = 10^8$ just crosses the zero line, giving rise to two points on the ceiling with zero velocity gradient – one corresponding to the point of separation and the other corresponding to the point of reattachment of the flow. A visual inspection of these curves is difficult, but the points of intersection of the curves with the zero

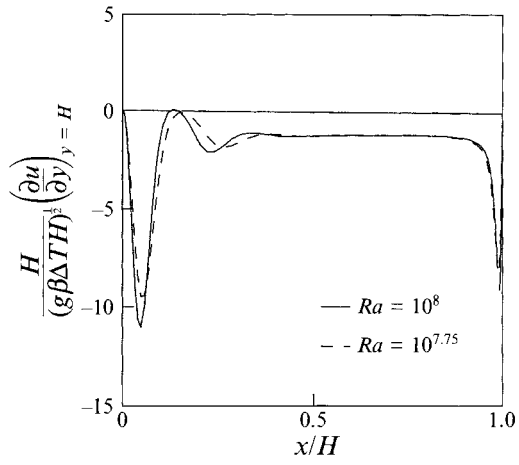

FIGURE 6. Determining commencement of separation: wall shear stress at the ceiling ($Pr = 1.2$).

line, if any, can be computationally determined. From figure 6, we can say that in the range of Ra values between $10^{7.75}$ and 10^8, there exists a value of Ra for which the velocity gradient curve just touches the zero line, giving rise to only one point of intersection. This value of Ra is the commencement point for separation. The range of Ra values of the probable range was narrowed down by making more computations, and the logarithmic mean of the narrowed-down range is taken as the point of commencement of separation. A least-squares fit was used to determine the power dependence of the commencement of separation on Prandtl number. The exponents of the Prandtl number obtained from the least-squares fit have been rounded off, and the constant of proportionality recomputed. The expressions so obtained are

$$Ra_s = \begin{cases} 10^{7.27} Pr^2 & \text{for } Pr \leqslant 1 \\ 10^{7.27} Pr^7 & \text{for } Pr \geqslant 1. \end{cases} \tag{4.2}$$

4.2. *Predicted scalings from hydraulic jump theory*

Paolucci & Chenoweth (1989) considered that the flow in the vertical boundary layer is turned due to the presence of the horizontal wall, and if the pressure in the corner could be assumed constant, then the flow at the mid-height of the enclosure could be used to characterize the horizontal flow that undergoes the sudden expansion. From the reasoning of Ivey (1984) and the computed results of Chenoweth & Paolucci (1986), they derived expressions for the characteristic velocity and depth of flow, just upstream of what they claimed to be the hydraulic jump, as follows:

$$\frac{\bar{v}}{v_B} = \begin{cases} 0.1298 & \text{for } Pr \leqslant 1 \\ 0.1298\ Pr^{-\frac{1}{2}} & \text{for } Pr > 1, \end{cases} \tag{4.3}$$

$$\frac{\Delta}{H} = \begin{cases} 2.145(Pr\ Ra)^{-\frac{1}{4}} & \text{for } Pr \leqslant 1 \\ 2.145 Ra^{-\frac{1}{4}} & \text{for } Pr > 1, \end{cases} \tag{4.4}$$

where $v_B = (g\beta\Delta TH)^{\frac{1}{2}}$, $\bar{v}$ is the mean velocity and Δ is the momentum thickness of the horizontal layer at mid-height of the vertical boundary layer. Equation (4.3) was derived by assuming that $\bar{v}$ represents the mean vertical velocity in the boundary layer at $y = H/2$. Paolucci & Chenoweth (1989) determined the mean velocity across the boundary layer of thickness δ, but they did not give a definition for δ. Equation (4.4) was derived by assuming that the momentum thickness of the horizontal layer

equals the vertical boundary layer thickness at $y = H/2$. This momentum thickness is defined as

$$\Delta = \frac{1}{v_{max}} \int_0^{H/2} v \, dx$$

and v_{max} is the maximum velocity in the vertical boundary layer. The dependence on Rayleigh number and Prandtl number is obtained using the boundary-layer scalings for the vertical boundary layer. The proportionality constants have been evaluated from the computational results of Chenoweth & Paolucci (1986). Following Ivey (1984), Paolucci & Chenoweth (1989) defined a characteristic Froude number F, given by

$$F = \frac{\bar{v}}{(g'\Delta)^{\frac{1}{2}}}, \tag{4.5}$$

where

$$g' = g\beta\Delta T/2, \tag{4.6}$$

which leads to the result

$$F = \begin{cases} 0.125(Pr\ Ra)^{\frac{1}{8}} & \text{for } Pr \leqslant 1 \\ 0.125 Pr^{-\frac{1}{2}} Ra^{\frac{1}{8}} & \text{for } Pr > 1. \end{cases} \tag{4.7}$$

This gives a unique value of Froude number for a given Rayleigh number, Prandtl number and aspect ratio. They used these expressions to compute the Froude number, and applied the hydraulic jump theory (Turner 1972) which predicts that for $1.0 < F < 1.3$, the jump dissipates energy in a stationary wavetrain, and remains at steady state, while for $F > 1.3$, the waves break and give rise to unsteady solutions. By this argument, they predicted that a hydraulic-jump-like structure must appear for Rayleigh numbers such that the corresponding Froude number exceeds unity, and the flow bifurcates to unsteadiness when the Froude number exceeds 1.3. These predictions can be summarized as

$$Ra > Ra_j = \begin{cases} 1.65 \times 10^7 Pr^{-1} & \text{for } Pr \leqslant 1 \\ 1.65 \times 10^7 Pr^4 & \text{for } Pr \geqslant 1 \end{cases} \tag{4.8}$$

for jumps to occur, and

$$Ra > Ra_b = \begin{cases} 1.34 \times 10^8 Pr^{-1} & \text{for } Pr \leqslant 1 \\ 1.34 \times 10^8 Pr^4 & \text{for } Pr \geqslant 1 \end{cases} \tag{4.9}$$

for a bifurcation to occur. For air in a square enclosure ($A = 1.0$; $Pr = 0.71$), the above equations predict $Ra_j = 2.32 \times 10^7$ and $Ra_b = 1.887 \times 10^8$. Henkes (1990) observed bifurcation at $Ra > 1.7$–1.75×10^8, while Chenoweth & Paolucci (1986) observed bifurcation at $Ra > 1.93 \times 10^8$ in their computed results.

As discussed earlier, the flow structure in the corner region of the enclosure shows two distinct phenomena: a recirculation region and flow separation with reattachment at the ceiling. Paolucci & Chenoweth (1989) do not clearly state which of these two they call the hydraulic jump. While they concentrated more on discussing the bifurcation of steady flow to a periodic flow, they made only a passing mention of what they called a hydraulic jump. They stated that the appearance of a hydraulic jump in the corner is characterized by steep large-amplitude waves and distinct recirculating regions at the horizontal walls. A sudden expansion in horizontal flow, which could have been referred to as the 'steep large amplitude waves' by Paolucci & Chenoweth (1989), appears at Rayleigh numbers as low as 10^5, while distinct

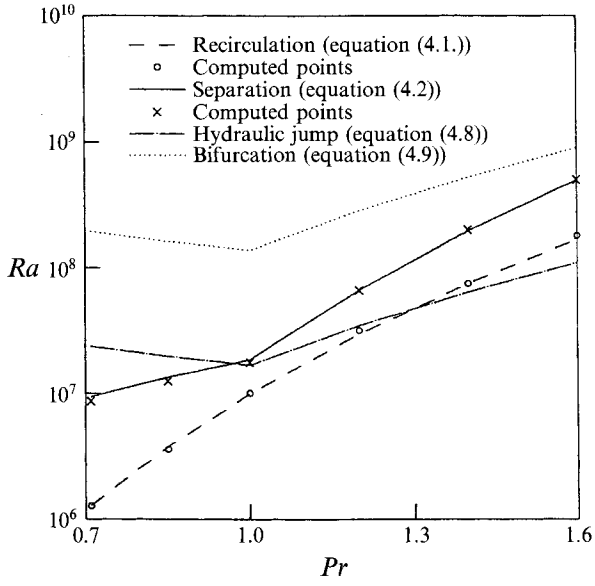

FIGURE 7. Scalings of corner phenomena.

recirculating regions at the horizontal walls appear only at Rayleigh numbers around 10^7. Thus, unfortunately, the definition of commencement of a hydraulic jump at $F = 1.0$ lacks precision; equation (4.8), which represents neither the commencement of recirculation nor that of separation, thus needs re-examination.

4.3. *Comparison of the scalings*

Figure 7 presents a comparison of the Rayleigh number of commencement of recirculation (Ra_r) given by (4.1), with that obtained from our numerical results, and the Rayleigh number of commencement of a hydraulic jump (Ra_j) predicted by (4.8). There are two distinct differences between (4.1) and (4.8). Firstly, (4.8) predicts a minimum in Ra_j at $Pr = 1.0$ whereas (4.1) shows a monotonic increase of Ra_r with Pr. Secondly, the exponent of Pr in (4.1) is 6, while those in (4.8) are -1 for $Pr \leqslant 1$ and 4 for $Pr \geqslant 1$. It can be seen that (4.1) fits all computed points very well.

Figure 7 also presents the Rayleigh numbers for the commencement of separation (Ra_s) defined by (4.2), with the computed values from our numerical results, and the hydraulic jump theory predictions (4.8). Here again, we observe that the power dependence derived from computed results for Ra_s is different from that for Ra_j predicted by hydraulic jump theory.

The prediction of the commencement of hydraulic jump and bifurcation to unsteadiness, (4.8) and (4.9), are also plotted for reference. This comparison demonstrates that the two phenomena observed in the corner region, which were originally interpreted as caused by an internal hydraulic jump, are indeed two distinct phenomena, and show different dependences on Rayleigh and Prandtl numbers. The observed dependences of these two phenomena are also different from those predicted by the theory of internal hydraulic jump.

It should be mentioned that the correlations presented here are derived from computed data over a limited range of Prandtl numbers, and are presented here only for the sake of comparison with the numbers predicted by Paolucci & Chenoweth (1989). However, the change in slope of the Ra_s curve at $Pr = 1$ shows qualitatively

that the asymptotic trends corresponding to $Pr \ll 1$ and $Pr \gg 1$ are felt even at Prandtl numbers close to unity.

5. Characterization of corner flow

In order to verify whether the corner flow is caused by a hydraulic jump, the flow in the corner region of the enclosure undergoing a sudden expansion needs to be characterized in terms of the governing parameters of a hydraulic jump. Since a typical internal hydraulic jump involves a stream undergoing an abrupt change of depth, let us identify the commencement of a hydraulic jump, if it exists, with the commencement of a change in the depth of the horizontal stream. A separation at the horizontal wall cannot be explained by classical theory of hydraulic jumps, and thus cannot be called a characteristic feature of the hydraulic jump.

It was shown that the global characterization of the corner phenomena to define a Froude number fails to represent the commencement of the change in depth of the stream. Instead of globally characterizing the corner phenomena in terms of the Rayleigh and Prandtl numbers, let us look at the horizontal stream which undergoes the sudden change of depth, and verify whether it can be characterized as a stream undergoing an internal hydraulic jump. In order to do this, we need to define the horizontal stream, and define its characteristic Froude number.

5.1. *Definition of local Froude numbers*

The Froude number of a given stream can be defined as

$$F = \frac{U}{(g'\Delta)^{\frac{1}{2}}}, \tag{5.1}$$

where U is the characteristic velocity of the stream, Δ is its characteristic depth, and g' is the effective gravitational acceleration based on the density differences in the stream (Turner 1972). In order to compute local Froude numbers, one needs to identify the characteristic velocity, density difference and depth, which appear in the definition of the Froude number F. Paolucci & Chenoweth (1989) used the values that are characteristic of the vertical boundary layer at mid-height of the enclosure. We could instead use the horizontal layer itself, and compute the characteristics of that layer, from the available numerical results.

In order to define the horizontal layer, we need to demarcate this layer from the rest of the flow. The dividing streamline (figure 3) is the obvious choice, since it clearly demarcates the wall layer from the interior flow. The flow between the streamline with the stream function $\psi = 0$ and the dividing streamline can be used as the wall stream. By definition, the enclosure walls have a stream function $\psi = 0$. When the flow separates at the horizontal wall, the horizontal layer is pushed away from the wall by the recirculating region at the wall, which is bounded by the streamline $\psi = 0$. It is more appropriate to consider the stream between the above recirculating region and the dividing streamline, when a separation occurs. In other words, when the flow shows a recirculation region at the corner and also separates at the wall, the stream in between the two recirculation regions is defined as the wall layer.

The wall layer defined above, in the region downstream of the turn at the corner, could be called the *horizontal layer*. For the horizontal layer, we can now define the characteristic velocity, depth and density difference. Since classical theory of hydraulic jumps is developed for an inviscid stream of uniform velocity and density, clearly demarcated from the surrounding fluid of a different density, we need to

define an equivalent stream to the horizontal layer, with uniform velocity and density. The equivalence can be determined by considering equal mass flow rates in the two streams. The alternatives available for the definition of the characteristic velocity are:

(i) the mean velocity of flow ($\bar{u}$) in the horizontal layer,

(ii) the maximum velocity of flow (u_{max}) in the horizontal layer and

(iii) the square root of the mean specific kinetic energy ($\overline{u^2}^{\frac{1}{2}}$) in the horizontal layer.

To decide on the most appropriate alternative to use, one must look at the fundamental definition of the Froude number. Critical flow ($F = 1.0$) is defined as a flow with a velocity equal to that of the infinitesimal long surface wave that can exist in that layer. If we consider the mean velocity $\bar{u}$ to represent the horizontal layer, then the thickness of the horizontal layer δ at the section of interest would be its characteristic depth. These quantities can be defined as

$$\left.\begin{aligned} U &= \bar{u} = \frac{1}{y_o - y_d}\int_{y_d}^{y_o} u \, \mathrm{d}y, \\ \Delta &= \delta = y_o - y_d, \end{aligned}\right\} \tag{5.2}$$

where y_d and y_o are the y-coordinates of the dividing streamline and the $\psi = 0$ streamline respectively, at the section of interest.

But there is a difficulty with this definition of characteristic velocity. Since part of the horizontal layer has velocities higher than the mean velocity, the flow can be locally supercritical even when the mean velocity defines the Froude number as unity or marginally less than unity. To overcome this difficulty, the alternative is to use the maximum velocity u_{max} in the cross-section. The corresponding depth of the stream, which satisfies conservation of mass in the layer, would then be the momentum thickness δ_m of the horizontal layer:

$$\left.\begin{aligned} U &= u_{max}, \\ \Delta &= \delta_m = \frac{1}{u_{max}}\int_{y_d}^{y_o} u \, \mathrm{d}y. \end{aligned}\right\} \tag{5.3}$$

Following the arguments of Turner (1972), the Froude number could be defined as follows:

$$F = \frac{1}{(g' \, \Delta / U^2)^{\frac{1}{2}}},$$

with the same notations as in (5.1). In this context, the characteristic velocity in the definition of the Froude number is the square root of the mean square velocity or the mean specific kinetic energy ($\overline{u^2}$). The corresponding depth is deduced by conservation of mass as follows:

$$\left.\begin{aligned} U &= u_{rms} = \left(\frac{1}{y_o - y_d}\int_{y_d}^{y_o} u^2 \mathrm{d}y\right)^{\frac{1}{2}}, \\ \Delta &= \delta_e = \frac{1}{u_{rms}}\int_{y_d}^{y_o} u \, \mathrm{d}y. \end{aligned}\right\} \tag{5.4}$$

Thus we have three alternative sets of definitions for the velocity scale U and length scale Δ in the definition of Froude number according to (5.1), as given by (5.2), (5.3) and (5.4). Paolucci & Chenoweth (1989) used the combination of $\bar{u}$ and δ_m, characteristic of the vertical boundary layer calculated at the mid-height of the enclosure, in their definition of Froude number.

The value of g' needs to be defined based on a characteristic density difference

between the layer and its ambient medium. This density difference depends directly on the characteristic temperature difference. Two of the alternatives available are

(i) the actual difference in temperature across the layer and

(ii) the difference between the bulk mean temperature of the layer and the bulk mean temperature of the ambient.

These two characteristic temperature differences and hence the characteristic g' read

$$\left.\begin{aligned} g' &= g\beta\,\Delta T, \\ \text{where} \quad \Delta T &= \Delta T_\ell = T(y = y_o) - T(y = y_d) \\ \text{or} \quad \Delta T &= \Delta T_b = \frac{\displaystyle\int_{y_d}^{y_o} uT\,\mathrm{d}y}{\displaystyle\int_{y_d}^{y_o} u\,\mathrm{d}y} - \frac{\displaystyle\int_{H/2}^{y_d} uT\,\mathrm{d}y}{\displaystyle\int_{H/2}^{y_d} u\,\mathrm{d}y}. \end{aligned}\right\} \tag{5.5}$$

In contrast to this, Paolucci & Chenoweth (1989) used the temperature difference between the hot vertical wall and the centre of the enclosure to define the Froude number.

Combining the various alternatives available for the velocity scale, length scale and the density difference, we obtain six alternative definitions of the local Froude number, which characterizes the horizontal layer as a stream undergoing an internal hydraulic jump in a surrounding medium:

$$F_1 = \frac{\bar{u}}{(g\beta\Delta T_\ell \delta)^{\frac{1}{2}}}, \tag{5.6}$$

$$F_2 = \frac{\bar{u}}{(g\beta\Delta T_b \delta)^{\frac{1}{2}}}, \tag{5.7}$$

$$F_3 = \frac{u_{max}}{(g\beta\Delta T_\ell \delta_m)^{\frac{1}{2}}}, \tag{5.8}$$

$$F_4 = \frac{u_{max}}{(g\beta\Delta T_b \delta_m)^{\frac{1}{2}}}, \tag{5.9}$$

$$F_5 = \frac{u_{rms}}{(g\beta\Delta T_\ell \delta_e)^{\frac{1}{2}}}, \tag{5.10}$$

$$F_6 = \frac{u_{rms}}{(g\beta\Delta T_b \delta_e)^{\frac{1}{2}}}. \tag{5.11}$$

The above discussion clearly shows the multiplicity of possibilities that exist to characterize the sudden expansion of the horizontal layer as a hydraulic jump. To illustrate further how arbitrary this characterization is, the six Froude numbers defined by (5.6)–(5.11) are plotted along the horizontal layer as a function of the streamwise coordinate in figure 8(*a*), for air at a Rayleigh number of 10^8. The curves show similar trends to each other, but the values of the Froude number determined by the various definitions are widely different.

Paolucci & Chenoweth (1989), on the other hand, used the boundary-layer equations characterizing the vertical boundary layer at mid-height of the enclosure to define the value of the Froude number that characterizes the flow globally. This, in fact, adds one more definition to the possible multiplicity of Froude-number definitions that can characterize a given flow situation.

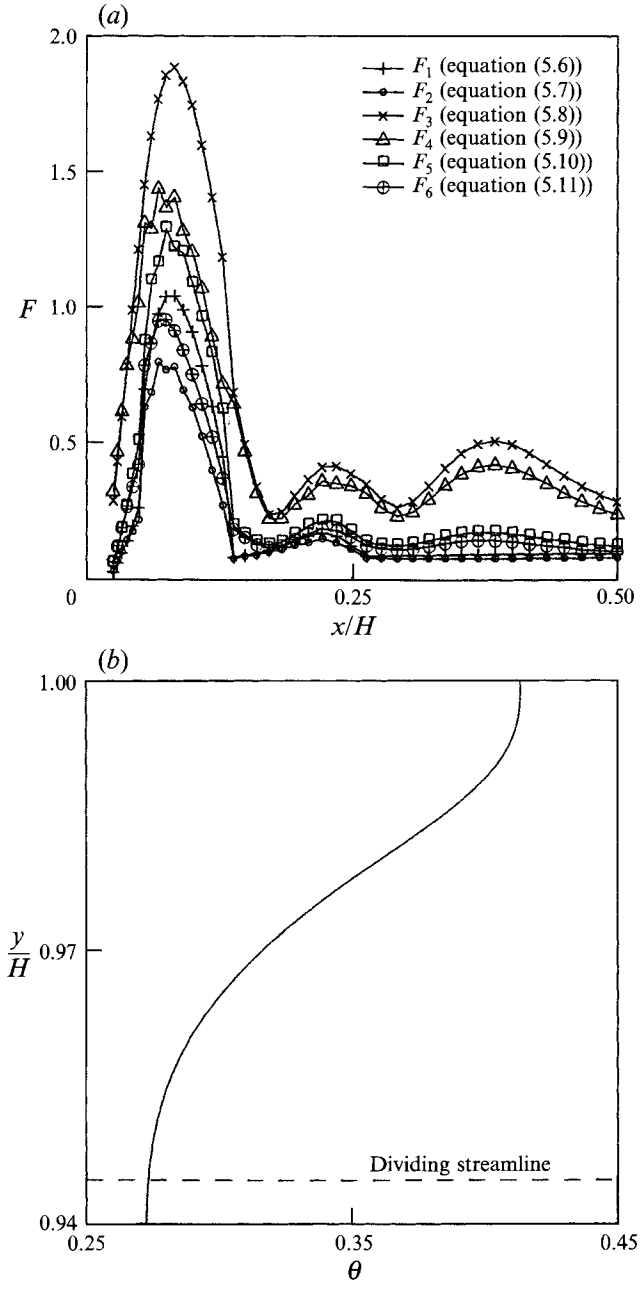

FIGURE 8. (*a*) Various Froude number definitions. (*b*) Temperature profile in horizontal layer ($Ra = 10^8$, $Pr = 0.71$).

Hence, a careful characterization of the wall layer undergoing the sudden expansion is essential. The six Froude-number definitions given by (5.6)–(5.11) are a first step in this direction. We should now choose from these definitions the most suitable one for the correct characterization of the sudden expansion in the corner region of an enclosure.

5.2. *Choice of the Froude-number definition*

In order to decide on the most suitable definition of Froude number corresponding to the problem under consideration, the theoretical analysis of flows with continuous density gradients by Long (1953, 1955) will be used. Long (1953) defined the Froude number as

$$F = \frac{\overline{U}}{\left(gH\dfrac{\Delta\rho}{\rho_b}\right)^{\frac{1}{2}}}, \tag{5.12}$$

where $\Delta\rho$ is the density difference across the depth H of the layer and ρ_b is the density at the bottom of the layer. Applying this definition to our case, we choose $\overline{u}$ as the characteristic velocity scale and δ as the depth scale, and the temperature difference across the layer (ΔT_ℓ) as the characteristic temperature difference. This gives the Froude number F_1 defined in (5.6).

Long (1955) discussed a difficulty he encountered in defining the value of $\Delta\rho$ in (5.12). He used a salt solution for his experiments, which had a finite density gradient in its interior, and almost zero density gradients near the surface and bottom. Using the density difference across the layer to define the Froude number, he found that the experimentally observed wave phenomena did not follow his theoretical predictions. When he instead used the mean gradient of the density in the interior of the layer, assuming that this mean gradient prevailed in the entire depth, in order to compute the characteristic density difference, the measured wavelengths agreed closely with the theoretically predicted wavelengths for that value of Froude number.

Figure 8(*b*) presents the temperature profile with the y-coordinate at a section close to the minimum cross-section of the horizontal layer, for a Rayleigh number 10^8 and Prandtl number 0.71. The temperature profile in the horizontal layer just upstream of the sudden expansion indeed resembles the density profile described by Long (1955). Thus, we choose to use the Froude number F_1 defined by (5.6) corrected as suggested by Long (1953) to represent the horizontal layer.

By the theoretical definition of Long (1953), if all streamlines in the stream coincide with an isotherm, then the critical Froude number in the case of no slip at the wall is determined to be $\frac{1}{3}$, and in the case of uniform velocity, its value is $1/\pi$. Long (1955) states that for his experimental cases, which were not strictly the same as his theoretical cases, the behaviour of the flow at the critical Froude number could not be verified owing to the uncertainty in the definition of the characteristic density difference. Nevertheless, the flow observed by Long (1955) in his experiments was quite close to that predicted by his theory. For our case, though the flow conditions are strictly not the same as the theoretical conditions of Long (1953, 1955), they are similar to his experimental conditions. Hence, by the arguments given above, we can expect that the critical Froude number for the present case is less than unity.

On the other hand, the critical Froude number of 1.0 is valid only for an inviscid stream of a homogeneous fluid, with no shear at the wall. As shown by Long (1953), for the flow of stratified fluids, the critical Froude number in the presence of wall shear is marginally higher than that in the absence of wall shear. Thus, we can expect the critical Froude number for our case to be less than unity owing to stratification, and its value can be expected to increase marginally owing to the presence of wall shear and the non-zero viscosity of the fluid. Since a critical Froude number of unity occurs only for homogeneous fluids with no viscosity or wall shear, to expect a hydraulic jump at $F > 1.0$ would be an oversimplification of the problem.

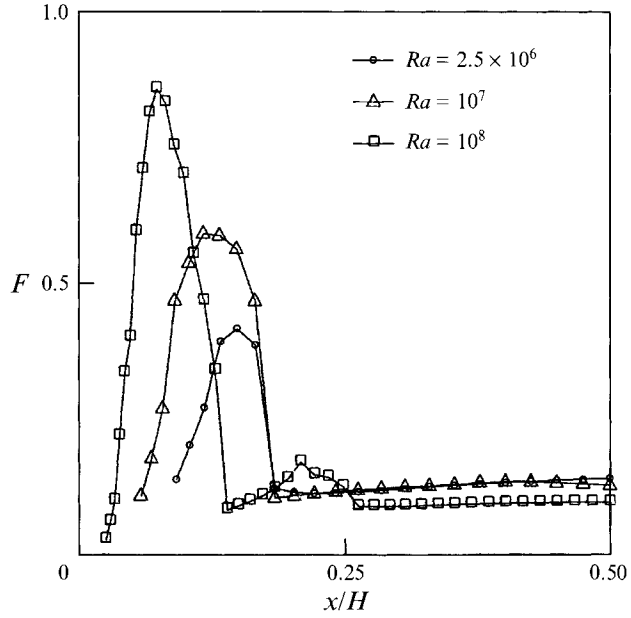

FIGURE 9. Local Froude number for different Rayleigh numbers ($Pr = 0.71$).

Figure 9 shows the plot of the streamwise variation of the Froude number F_1 corrected as suggested by Long (1955), in the upper left quarter of the enclosure, for $Ra = 2.5 \times 10^6$, 10^7 and 10^8, at $Pr = 0.71$. It can be seen that there is an abrupt change in Froude number in all the curves even when it does not exceed 1.0. This shows that the phenomenon causing the sudden expansion in the corner region of an enclosure is not a simple internal hydraulic jump.

6. Verification of jump behaviour

By the theory of hydraulic jumps, the flow shows no change in depth when it is subcritical or critical, but a jump is possible only when it becomes supercritical. It does not allow for a gradual change in the depth ratio across the jump. When the flow is supercritical, the relation between the upstream depth y_1 and the downstream depth y_2 is a unique function of the Froude number, given as follows:

$$\frac{y_2}{y_1} = \frac{1}{2}\left((8F^2 + 1)^{\frac{1}{2}} - 1\right) \qquad \text{for } F \geqslant 1. \tag{6.1}$$

In the case of the flow of air in an enclosure, however, the flow spreads out into the core of the enclosure even at Rayleigh numbers as low as 10^5, as discussed earlier. If the hypothesis that the expansion in flow is due to a hydraulic jump is valid, the flow must become supercritical for Rayleigh numbers as low as 10^5, well below the value of Ra_j predicted by (4.8).

The ratio of the downstream depth of the stream to the upstream depth is a characteristic feature of hydraulic jumps, which could be used to correlate the present problem with hydraulic jumps. Since the expression for conjugate relationship given by (6.1) for a simple hydraulic jump is derived from basic equations of conservation of mass and momentum, and the computed flow field is also a solution of the conservation equations of mass and momentum, a direct comparison of the two

Ra	$F_{3,max}$	$\frac{y_2}{y_1}$ (equation (6.1))	$\frac{y_2}{y_1}$ (computations)
2.5×10^6	0.951	-	2.277
10^7	1.135	1.181	3.156
$10^{7.25}$	1.213	1.287	3.586
$10^{7.875}$	1.540	1.735	4.648
10^8	1.853	2.168	4.859

TABLE 1. Depth ratios across a sudden expansion

cases is possible. Since the wall layer represents the flow between two streamlines, mass conservation is taken care of, while momentum conservation follows from the governing Navier–Stokes equations. The basic difference between the present case and (6.1) is that (6.1) is derived for an inviscid flow of a homogeneous fluid, while the present case is the viscous flow of a fluid with density variation. Table 1 compares the values of y_2/y_1 predicted by (6.1) for the peak Froude number F_3 (equation (5.8)) in the horizontal layer corresponding to the given Rayleigh number with those observed from the flow field. It can be clearly seen that the values of the observed ratios are much higher than those predicted. Here, the definition of F_3 is used for the comparison, because the characteristic Froude number according to this definition predicts the highest value of the ratio of depths presented in table 1. The other definitions predict even lower values. In particular, the definition F_1 corrected according to Long (1955) predicts that the Froude number for all the Rayleigh numbers considered is less than unity. It is clear from the above comparison that the depth ratio in the enclosure flow does not follow the conjugate relation for a hydraulic jump, given by (6.1), for any of the definitions of Froude number given by (5.6)–(5.11).

7. Energy considerations

A hydraulic jump is known to be essentially associated with energy loss. There exists no definite expression in the literature for energy losses downstream of a hydraulic jump of a fluid with arbitrarily specified density profiles. But it is possible, however, to verify whether there is a loss of mechanical energy at the observed sudden expansion. A hydraulic jump is always associated with loss of mechanical energy, even when the flow is inviscid. If there is no abrupt loss in mechanical energy at the sudden expansion, this would be conclusive evidence that the observed sudden expansion is not a hydraulic jump.

In order to examine the flow in the corner region of the enclosure for energy losses across the sudden expansion, it is necessary to derive an equation governing the transport of mechanical energy in the enclosure. The equation of mechanical energy conservation can be deduced from the momentum equations (2.2) and (2.3) and written as follows:

$$\underbrace{\left(\frac{\partial}{\partial t}+u\frac{\partial}{\partial x}+v\frac{\partial}{\partial y}\right)\left(\frac{u^2+v^2}{2}\right)}_{(I)} \quad + \quad \underbrace{\left(u\frac{\partial}{\partial x}+v\frac{\partial}{\partial y}\right)\left(\frac{p_d}{\rho_{ref}}\right)}_{(II)} \quad - \quad \underbrace{g\beta v(T-T_{ref})}_{(III)}$$

$$= \nu \left(\frac{\partial^2}{\partial x^2} + \frac{\partial^2}{\partial y^2}\right)\left(\frac{u^2+v^2}{2}\right) \quad - \quad \nu\left[\left(\frac{\partial u}{\partial x}\right)^2 + \left(\frac{\partial v}{\partial y}\right)^2 + \left(\frac{\partial v}{\partial x}\right)^2 + \left(\frac{\partial u}{\partial y}\right)^2\right]. \tag{7.1}$$
$$(IV) \qquad\qquad (V)$$

Term (I) in (7.1) represents the convective transport of kinetic energy, terms (II) and (III) represent the pressure and buoyancy contributions to the potential energy, term (IV) represents the viscous diffusion of kinetic energy and term (V) represents the dissipation of the mechanical energy of the flow, constituted by the kinetic and potential energy terms given above, due to viscosity. If there are losses associated with the sudden expansion in the corner region of the flow, the loss of mechanical energy of the flow has the form of energy dissipation due to viscosity. Thus, any loss of energy must be reflected in the viscous terms of (7.1). Figure 10(*a*) shows the contours of the viscous terms $(IV + V)$ of (7.1) as calculated for air at $Ra = 10^8$. It can be seen that the viscous terms make a significant contribution to (7.1) only in the vertical boundary layers. It is more relevant, however, to check the relative importance of the viscous terms, as compared to the rest of the terms in the equation, in the various regions in the enclosure. The relative magnitude of the viscous terms as labelled in (7.1) can be defined as

$$\text{Relative magnitude of losses} = \frac{|IV + V|}{|I| + |II| + |III| + |IV + V|}. \tag{7.2}$$

Figure 10(*b*) shows the relative magnitude of viscous terms in the enclosure at $Ra = 10^8$. It is seen that this relative magnitude is significant only in the boundary layers close to the vertical walls where the gradients of velocity are large, and at the top right and bottom left corners, where the flow velocities are so small that the terms (I), (II) and (III) are also as small as the viscous terms. In that part of the top left and bottom right corners, where the sudden expansion is observed, no significant losses occur. This implies that this sudden expansion in the flow is not associated with mechanical energy loss due to viscosity. This absence of energy loss proves conclusively that the sudden expansion observed in the corner region of an enclosure is not associated with an internal hydraulic jump phenomenon.

8. Thermal mechanism of the corner structure

It was established in the previous sections that the corner flow structure is not caused by an internal hydraulic jump: such a jump is a hydrodynamic mechanism. In this section, the thermal mechanisms which may cause this structure are examined. The temperature field in the boundary layer and corner regions is examined with reference to the thermal stratification in the core region to seek an explanation of the observed behaviour of the corner flow.

8.1. *Mechanism of separation at the ceiling*

Figure 11(*a*) shows the isotherms for air at $Ra = 10^8$ in the upper left quarter of the enclosure. The isotherms indeed reflect the various asymptotic structures: a thin vertical boundary layer, horizontal boundary layer, a corner region and a core region. The core region is characterized by a stable stratification: i.e. the temperature is only a function of y, and increases with increase in y. If we examine the temperature levels at each y in the boundary layer in comparison with the

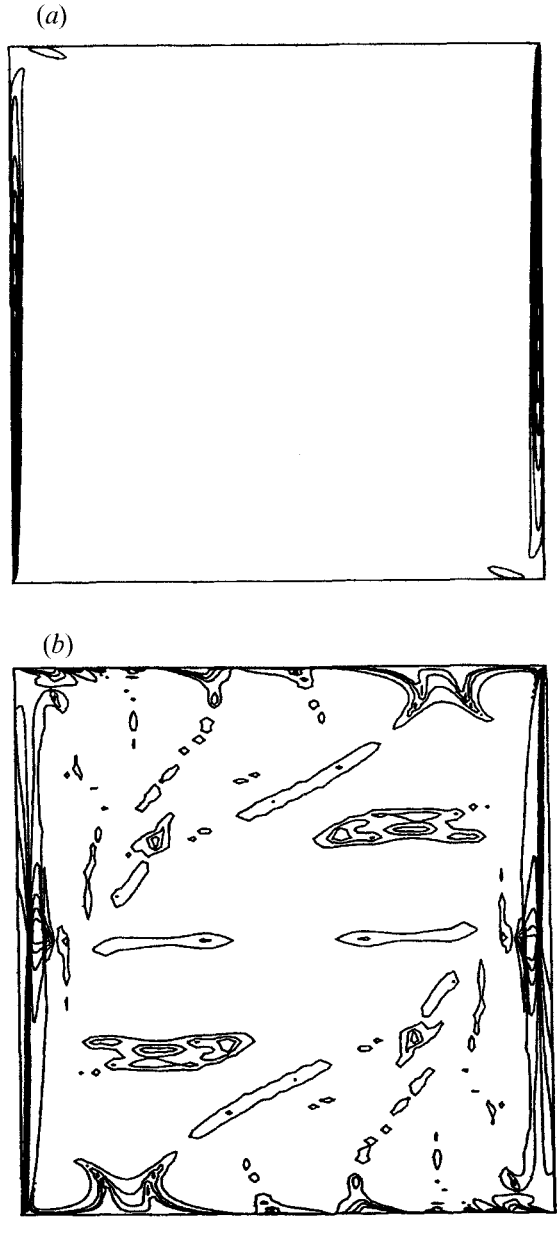

FIGURE 10. (*a*) Contours of viscous term. (*b*) Contours of relative magnitude of viscous terms ($Ra = 10^8$, $Pr = 0.71$).

corresponding value in the core, we find that the non-dimensional temperature does not fall from $\theta = 0.5$ at the hot wall to the corresponding value in the core monotonically. The temperature falls below that of the core (an *undershoot*), and then reaches the core value oscillatorily. Such an oscillatory structure is also found in the streamlines, showing reversal of flow in the outer part of the vertical boundary layer (figure 11*b*). Cheesewright (1967), Yang, Novotny & Cheng (1972) and Henkes & Hoogendoorn (1989) observed such temperature variations in the similarity solutions of the boundary-layer equations for natural convection over a vertical hot plate in

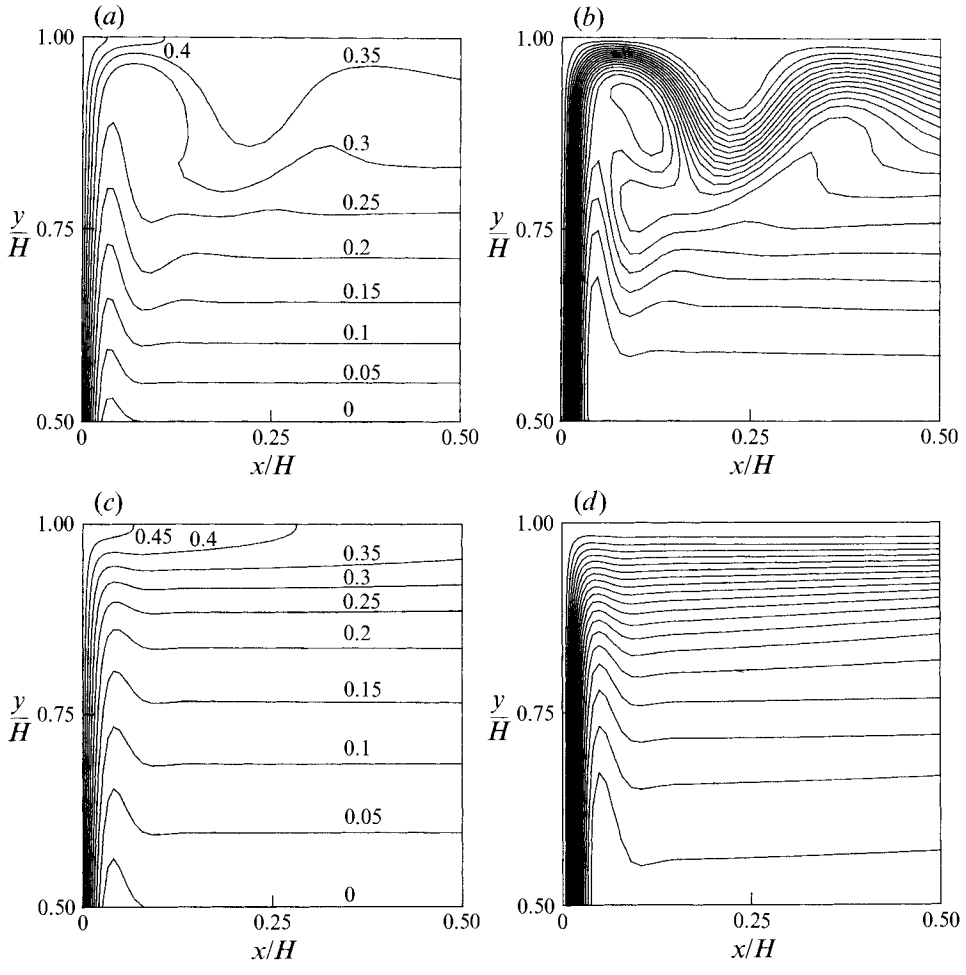

FIGURE 11. (*a*) Isotherms in upper left quarter of the enclosure: $Ra = 10^8$; $Pr = 0.71$. (*b*) Streamlines in upper left quarter of the enclosure: $Ra = 10^8$; $Pr = 0.71$. (*c*) Isotherms in upper left quarter of the enclosure: $Ra = 10^8$; $Pr = 70$. (*d*) Streamlines in upper left quarter of the enclosure: $Ra = 10^8$; $Pr = 70$.

a stably stratified environment. Cheesewright (1967) explains the physical reason for the undershoot-overshoot oscillation as 'the rate of heat transfer from the plate to the fluid in the outer part of the boundary layer is not sufficient to keep its temperature in step with the temperature outside the boundary layer'. The damped oscillation structure of isotherms in figure 11(*a*) is quite similar to that observed in the vertical boundary layers investigated in the above references.

Close to the ceiling, these under- and overshoots in the temperature field are affected by the presence of the top wall. This is seen clearly by comparing the shapes of the isotherms of $\theta = 0.25$, 0.3 and 0.35 in figure 11(*a*). While the $\theta = 0.25$ isotherm freely oscillates to attain its core level, the $\theta = 0.35$ isotherm is not able to freely oscillate above its level in the core. The overshoot in y-coordinate of the isotherms above their levels in the core are $0.116H$, $0.135H$ and $0.033H$ for the $\theta = 0.25$, 0.3 and 0.35 isotherms respectively. Since the θ value of the ceiling at $x = H/2$ is about 0.36, there are no over- or undershoots observed for isotherms corresponding to $\theta > 0.36$.

But the isotherms in the range of $\theta = 0.3$–0.35 are significantly above their core levels as they turn the corner, and hence experience a force of (negative) buoyancy, forcing them downwards. This results in the bulk of the horizontal flow in this temperature range coming down in the form of a buoyant plume. At high Rayleigh numbers, the strength of the downward flow of the plume and its entrainment are so strong that the flow separates from the ceiling. This can be seen by comparing the streamlines in figure 11(*b*) with the isotherm plot in figure 11(*a*). The shapes of the isotherms in the range $\theta = 0.3$–0.35 and the streamlines are quite similar, implying that the effect of viscosity and diffusion of heat are negligible in this region. As the flow progesses towards the core, the layer $\theta = 0.3$–0.35 also becomes thicker from about $0.014H$ near the corner to about $0.115H$ at $x = H/2$. The downward plume flow and the resulting entrainment causes separation of the flow at the ceiling, and the oscillatory attainment of the core temperature allows the reattachment.

8.2. *Effect of Prandtl number*

Figures 11(*c*) and 11(*d*) present the isotherms and streamlines in the upper left quarter of the enclosure for $Pr = 70$, at $Ra = 10^8$. The temperature levels of the stratified core are quite different in this case as compared to those for air, shown in figure 11(*a*). The isotherms are quite sparsely distributed in the central region of the core ($y = 0.5H$–$0.75H$), while they are quite close together near the horizontal wall. This results in quite small over- and undershoots in isotherms at the edge of the boundary layer, and hence there is no strong plume. Therefore, there is no separation of flow at the ceiling at this Prandtl number.

8.3. *Asymptotic theory and finite-Prandtl-number effects*

From the above discussion it is clear that the temperature distribution in the core region determines whether or not the flow separates in the corner region. But, this temperature distribution in the corner region itself is determined by the equilibrium between the vertical boundary layer flow and the horizontal core flow. The difficulty in the present analysis is that an asymptotic theory to predict the flow structure as $Ra \rightarrow \infty$ at all Prandtl numbers does not exist. Such a theory should describe how the flow structures, viz. the vertical boundary layers, core, horizontal boundary layers and corners should match. It should also be able to predict whether there exists a hierarchical ordering of these different structures. If such a hierarchy indeed exists, then we can explain the corner phenomena in terms of cause and effect.

Gill (1966) assumed that there exists a hierarchy of flow structures at asymptotically high Rayleigh numbers at all Prandtl numbers, which comprises only two generic regimes: the vertical boundary layer and the core. The horizontal boundary layer and the corner region, which result from no-slip conditions at the solid walls, can be derived from the asymptotic structures of the core and the vertical boundary layer. As $Ra \rightarrow \infty$, negligible mass flows through the horizontal boundary layer, and the vertical boundary layer comes into equilibrium with the core. The role of stratification is to tune the horizontal mass flow in the core, which is also the in- and outflow of mass to the vertical boundary layers, to their equilibrium levels.

This theory appears to be valid in both cases discussed in §§8.1 and 8.2, in the respect that the stratification in the core region determines the in- and outflow of mass to the vertical boundary layer. Gill (1966) derived the particular case of asymptotic solutions for high Prandtl numbers, and predicted the stratification in the core for these Prandtl numbers as $Ra \rightarrow \infty$. The approximate solutions of the asymptotic system by Gill (1966) predicted a stratification $S = [(\partial T/\partial y)(H/\Delta T)]_c$ at the centre

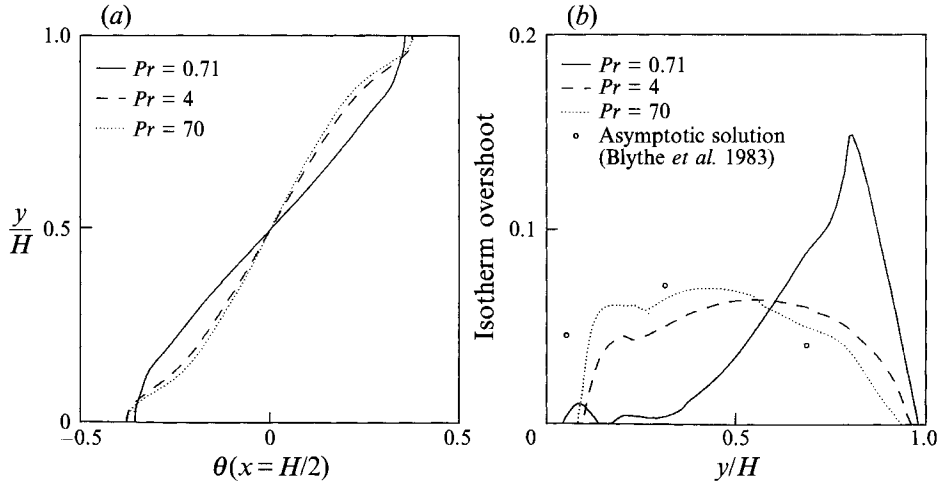

FIGURE 12. (*a*) Temperature profiles at $x = H/2$. (*b*) Isotherm overshoot in the boundary layer.

of the enclosure to be 0.42, while an accurate solution of the same system by Blythe, Daniels & Simkins (1983) predicts its value to be 0.52. The present solution of Navier–Stokes equations for $Pr = 70$ also yields $S = 0.52$ for $Ra = 10^8$.

It was shown in §3.2 that the separation at the ceiling vanishes at $Pr = 1.4$ for $Ra = 10^8$. This means that the core stratification changes drastically between $Pr = 0.71$ and $Pr = 1.4$. Figure 12(*a*) shows the temperature profiles at $x = H/2$ for $Ra = 10^8$ at Prandtl numbers 0.71, 4.0 and 70.0. The curves show that the core stratification changes very little between $Pr = 4$ and $Pr = 70$, and all the change in core temperature distribution takes place at $Pr < 4.0$. The temperature profiles at $x = H/2$ for $Pr = 70$ matches closely with the asymptotic core temperature profile presented by Blythe *et al.* (1983). Figure 12(*b*) shows the overshoot distance of the isotherms over their position at $x = H/2$, as a function of their y-coordinate at $x = H/2$, for the above values of Prandtl number. The overshoots measured from one of the figures presented in the asymptotic solution of Blythe *et al.* (1983) are also shown in figure 12(*b*). This figure shows how intimately the isotherm overshoots are related to the centreline temperature distribution, and how much the overshoot affects the corner flow structure. For $Pr > 4.0$, the overshoot declines to zero gradually, with maxima in the lower half of the hot vertical wall. These overshoot values agree quite well with the asymptotic solution of Blythe *et al.* (1983). At lower Prandtl numbers, however, the overshoots are largest close to the ceiling, and the decline to zero is abrupt, as the flow encounters the ceiling. The asymptotic structure of the core and the vertical boundary layer is no longer similar to that predicted by the asymptotic solutions which are valid for large Prandtl numbers.

Therefore, an asymptotic theory which predicts the core structure at these Prandtl numbers as $Ra \rightarrow \infty$ is essential, based on which we can explain the behaviour of the corner flow. Unfortunately, there exists no such asymptotic theory for finite Prandtl numbers. Only Graebel (1981) has presented some approximate solutions, in which he has neglected some terms in the equations. For air, his prediction is $S = 0.49$, which is considerably lower than the value $S = 0.99$ predicted by Navier–Stokes computations. This strongly suggests that the approximations made by Graebel (1981) impair the reliability of the results. Hence, there is a need for an asymptotic theory to predict

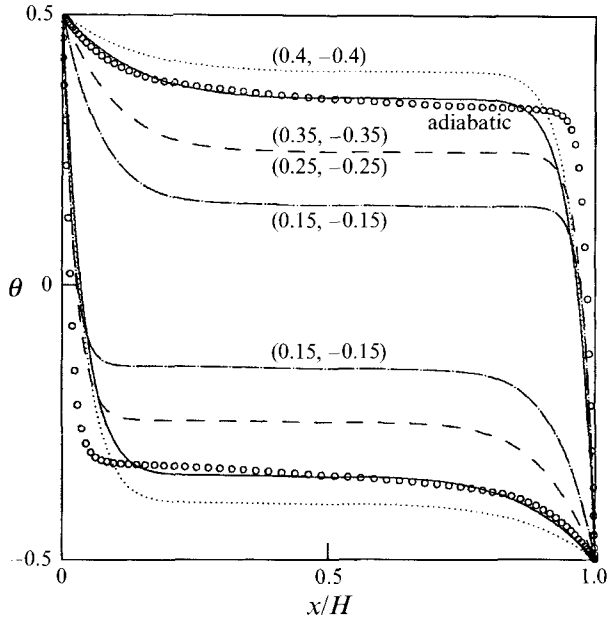

FIGURE 13. Temperature profiles on the horizontal walls: the top and bottom wall temperatures at $x = H/2$ are shown on the curves ($Ra = 10^7$, $Pr = 0.71$).

the core structure as $Ra \to \infty$ at finite Prandtl numbers, to enable us to predict the Prandtl-number dependence of the core flow, and hence the corner structure.

8.4. *Mechanism of recirculation*

The downward plume from the ceiling and the vertical boundary layer both can entrain fluid along their edge. When they come close to each other, part of the downward plume is re-entrained into the vertical boundary layer and vice-versa, resulting in a recirculating pocket of fluid between the two streams. The mechanism of this re-entrainment is independent of the mechanism of separation from the ceiling, and hence the difference in the dependencies of the two flow structures on Rayleigh and Prandtl numbers.

8.5. *Effect of horizontal wall temperature on corner flow*

We now know that the corner flow structure is governed by the temperature distribution in the core. This temperature distribution can be locally altered by varying the temperature of the horizontal walls. Computations were carried out with different thermal boundary conditions, other than adiabatic horizontal walls. Figure 13 shows the non-dimensional temperature distribution (θ) along the adiabatic horizontal walls for $Ra = 10^7$ and $Pr = 0.71$ (shown by circles). It can be seen that except close to the corners, at the top wall θ is nearly constant at around 0.35, while at the bottom wall θ is around -0.35. Temperature profiles similar in shape to the adiabatic wall temperature profile were generated using suitable functions, and used as boundary conditions for the computations. These temperature profiles are also shown in figure 13. The top and bottom horizontal wall temperatures were maintained at (0.5, −0.5), (0.4, −0.4), (0.35, −0.35), (0.25, −0.25), and (0.15, −0.15) respectively for the different computations, except near corners. The resulting streamline patterns for $Ra = 10^7$ and $Pr = 0.71$ are presented in figure 14(*a–f*).

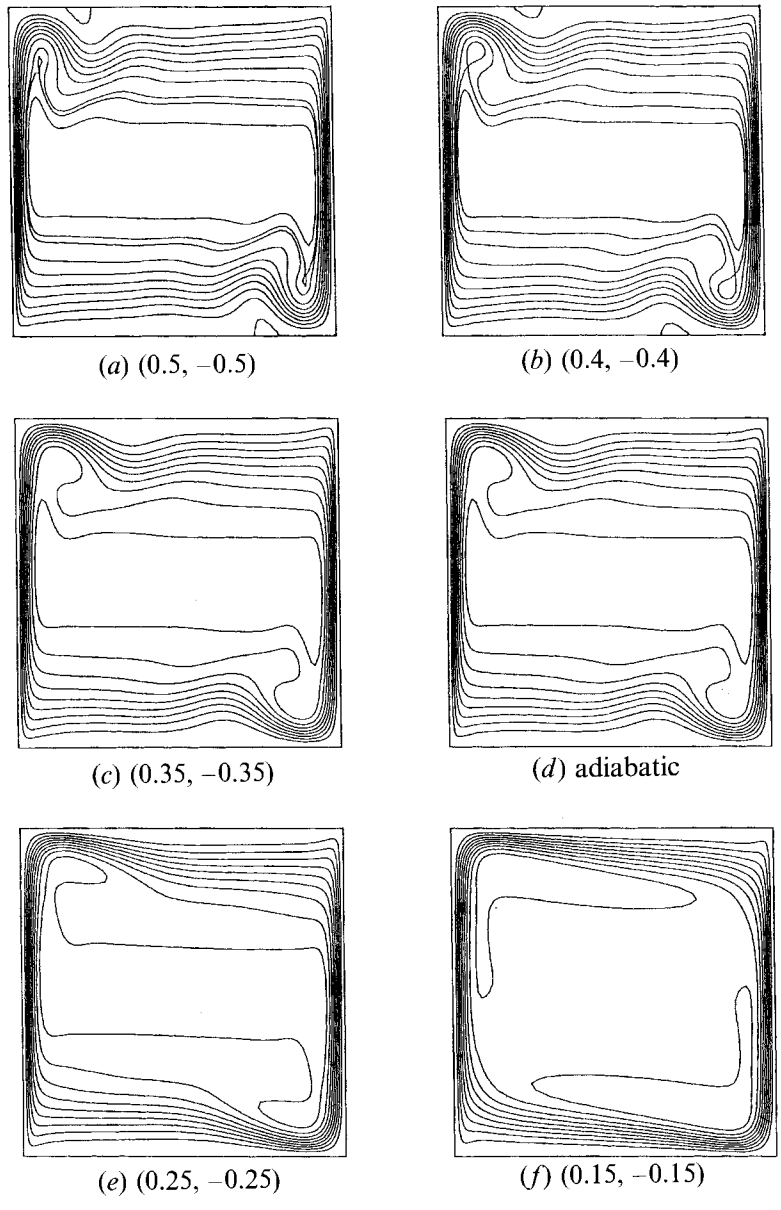

FIGURE 14. Effect of boundary conditions on flow structures: streamlines for the profiles shown in figure 13.

Figure 14(*d*) presents the adiabatic wall case, and figure 14(*c*) presents the case corresponding to (0.35, −0.35) boundary conditions. It can be seen that these two figures look very much alike, in spite of the minor differences between the shapes of their temperature profiles at the horizontal walls. Figures 14(*a*) and 14(*b*) present the cases of (0.5, −0.5) and (0.4, −0.4) respectively, where the top wall is hotter (and the bottom wall is cooler) than the adiabatic case. These figures show that the separation zone at the horizontal wall becomes more pronounced when the mean temperature of the top wall increases (and that of the bottom wall decreases), while the recirculation zone becomes less pronounced. On the other hand, in figures 14(*e*) and 14(*f*), which

show the cases of (0.25, −0.25) and (0.15, −0.15) respectively, we find the reverse: the separation at the horizontal wall is less favoured, while the recirculation zone in the corner becomes larger, as the mean temperature of the top wall decreases (and that of the bottom wall increases).

9. Conclusions

The present work closely examined the flow structures observed in the corner region of a square enclosure with differentially heated vertical walls and adiabatic horizontal walls. The principal aim was to examine whether these flow structures are indeed caused by an internal hydraulic jump, as suggested in literature. It was found that the corner flow structure has no connections with a hydraulic jump phenomenon.

(i) The corner flow phenomena are constituted of two distinct features, viz. a recirculation and a separation at the horizontal wall. The scalings of these two features are different from one another, and from that predicted by the theory of internal hydraulic jumps.

(ii) The theory of the internal hydraulic jump does not explain the separation of flow at the ceiling of the enclosure.

(iii) A multiplicity of possible Froude-number definitions exists, which give rise to widely different values of Froude number for the same flow situation. This demonstrates the arbitrary nature of Froude-number definition.

(iv) Since the stream under consideration has continuous density and velocity variations across it, the critical Froude number for this flow is not equal to unity. The plot of streamwise Froude number indicates the occurrence of a jump at Froude number less than unity. Hence, the proposition that a hydraulic jump commences at $F = 1.0$ and breaks up at $F = 1.3$ appears to be an oversimplification of a complex problem.

(v) According to the theory of hydraulic jumps, a change in depth of the stream is possible only when the characteristic Froude number exceeds the critical value. Unlike a typical internal hydraulic jump, in which the change in depth commences abruptly when the flow becomes supercritical, the spreading of the horizontal layer in an enclosure commences as a gradual expansion at low Rayleigh numbers and becomes sharper as the Rayleigh number increases. Equation (4.8) based on the hydraulic jump theory does not represent the starting point of the expansion of the horizontal flow, but the expansion of flow is observed even at Rayleigh numbers lower than that predicted by this equation.

(vi) The depth ratio of the expanding enclosure flow does not agree with the relation of conjugate depths, which characterizes a simple hydraulic jump.

(vii) The equation of conservation of mechanical energy shows that this expansion is not associated with any loss of energy.

(viii) Thus, we conclude that the phenomena observed in the corner region of an enclosure at high Rayleigh numbers are not related to an internal hydraulic jump. It appears that equation (4.9) due to Paolucci & Chenoweth (1989) predicted the bifurcation to unsteady flow for air reasonably well only as a matter of coincidence.

(ix) It has been qualitatively shown in this paper that the corner structure is caused solely by thermal effects. The stable core stratification causes a temperature undershoot in the vertical boundary layer. This results in colder fluid than the stratified core reaching the ceiling, and the resulting force of buoyancy causes a plume. The flow separates from the ceiling when this plume grows strong, with

increase in Rayleigh number. Recirculation is caused by re-entrainment of this plume into the vertical boundary layer.

(x) At higher Prandtl numbers, the core temperature distribution does not allow large undershoots of temperature, and hence there is no recirculation or separation at the corner.

The authors thank Delft University of Technology and the Royal Netherlands Academy of Arts and Sciences, for providing the necessary funding to perform this research.

REFERENCES

ARMFIELD, S. W. & PATTERSON, J. C. 1991 Direct simulation of wave interactions in unsteady natural convection in a cavity. *Intl J. Heat Mass Transfer* **34**, 929–940.

BLYTHE, P. A., DANIELS, P. G. & SIMKINS, P. G. 1983 Thermal convection in a cavity: the core structure near the horizontal boundaries. *Proc. R. Soc. Lond.* **A 387**, 367–388.

CHEESEWRIGHT, R. 1967 Natural convection from a plane, vertical surface in non-isothermal surroundings. *Intl J. Heat Mass Transfer* **10**, 1847–1859.

CHENOWETH, D. R. & PAOLUCCI, S. 1986 Natural convection in an enclosed vertical air layer with large horizontal temperature differences. *J. Fluid Mech.* **169**, 173–210.

GILL, A. E. 1966 The boundary layer regime for convection in a rectangular cavity. *J. Fluid Mech.* **26**, 515–536.

GRAEBEL, W. P. 1981 The influence of Prandtl number on free convection in a rectangular cavity. *Intl J. Heat Mass Transfer* **24**, 125–131.

HENKES, R. A. W. M. 1990 Natural convection boundary layers. PhD thesis, Delft University of Technology, Delft, the Netherlands.

HENKES, R. A. W. M. & HOOGENDOORN, C. J. 1989 Laminar natural convection boundary layer flow along a vertical heated plate in a stratified environment. *Intl J. Heat Mass Transfer* **32**, 147–155.

HENKES, R. A. W. M. & HOOGENDOORN, C. J. 1990 On the stability of natural convection flow in a cavity heated from the side. *Appl. Sci. Res.*, **47**, 195–220.

IVEY, G. N. 1984 Experiments on transient natural convection in a cavity. *J. Fluid Mech.* **144**, 389–401.

JANSSEN, R. J. A. & HENKES, R. A. W. M. 1993 Accuracy of finite-volume discretizations for the bifurcating natural-convection flow in a heated square cavity. *Numer. Heat Transfer* B **24**, 191–207.

LE QUÉRÉ, P. 1991 Accurate solutions to the square thermally driven cavity at high Rayleigh number. *Comput. Fluids* **20**, 29–41.

LE QUÉRÉ, P. 1987 Étude de la transition à l'instationnarité des écoulements de convection naturelle en cavité verticale différentiellement chauffée par méthodes spectrales Chebyshev. Thèse d'Etat, University of Poitiers, France.

LONG, R. R. 1953 Some aspects of the flow of stratified fluids. 1. A theoretical investigation. *Tellus* **5**, 42–58.

LONG, R. R. 1955 Some aspects of the flow of stratified fluids. 3. Continuous density gradients. *Tellus* **7**, 341–357.

PAOLUCCI, S. & CHENOWETH, D. R. 1989 Transition to chaos in a differentially heated vertical cavity. *J. Fluid Mech.* **201**, 379–410.

PATTERSON, J. C. & ARMFIELD, S. W. 1990 Transient features of natural convection in a cavity. *J. Fluid Mech.* **219**, 469–497.

TURNER, J. S. 1972 *Buoyancy Effects in Fluids.* Cambridge University Press.

VAHL DAVIS, G. DE 1983 Natural convection of air in a square cavity: A benchmark numerical solution. *Intl J. Numer. Meth. Fluids* **3**, 249–264.

YANG, K. T., NOVOTNY, J. L. & CHENG, Y. S. 1972 Laminar free convection from a nonisothermal plate immersed in a temperature stratified medium. *Intl J. Heat Mass Transfer* **15**, 1097–1109.